Comparison of Oxidizing Agents for the Oxidative Coupling of Methane over State-of-the-Art Catalysts

K. Langfeld[1], B. Frank[2], V. E. Strempel[1], C. Berger-Karin[3], G. Weinberg[2], E. V. Kondratenko[3], R. Schomäcker[1,*]

[1]Institute of Chemistry, Technical University Berlin, Straße des 17. Juni 124, 10623 Berlin, Germany

[2]Department of Inorganic Chemistry, Fritz Haber Institute of the Max Planck Society, Faradayweg 4-6, 14195 Berlin, Germany

[3]Leibniz Institute for Catalysis at the University of Rostock, Albert-Einstein-Straße 29a, 18059 Rostock, Germany

[*] Corresponding author: e-mail schomaeker@tu-berlin.de,

Abstract

The synthesis of selected state-of-the-art catalysts providing high performances in the oxidative coupling of methane (OCM) with O_2 was reproduced according to the respective methods reported in literature. A reference material with identical stochiometric composition was further synthesized by applying the cellulose templating (CT) method. This method increases the surface area and affects the phase composition and crystallite size of the catalysts as determined by N_2-physisoprtion, X-ray diffraction (XRD), and scanning electron microscopy. This, however, is in most cases detrimental to the catalytic OCM performance due to enhanced global activity resulting in hot spots in the catalyst bed. Prepared catalysts were tested in the OCM under variation of temperature (973–1073 K), GHSV (3,600–100,000 h^{-1}) and oxidizing agent (O_2 and N_2O). In general, conversions of CH_4 when using N_2O are lower than in the presence of O_2, however, the selectivities to C_2 products ethane and ethylene are higher even at a similar level of CH_4 conversion. This confirms the presence of different oxygen species formed by activation of these oxidizing agents.
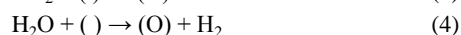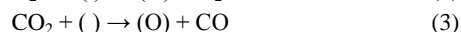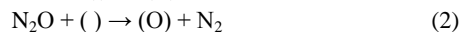
1. Introduction

The use of methane as a chemical feedstock and its transformation into higher hydrocarbons has been the focus of a number of research efforts for several decades. With increasing oil prices especially the Fischer-Tropsch (FT) process via synthesis gas, which is obtained, e.g., by steam reforming of methane, actually retrieves a lot of attractiveness. However, one drawback with regard to process costs is the need for two individual reactors to consecutively produce synthesis gas and higher hydrocarbons or alcohols. Even more complex is the route to high-value olefins via methanol, which is synthesized from synthesis gas. A highly attractive one-step transformation is the oxidative coupling of methane (OCM) to C_2 (C_2H_6 and C_2H_4) hydrocarbons ethane and ethylene discovered in the early 1980's

[1]. This reaction, even though extensively investigated and optimized for almost three decades, provides low C_2 selectivities at high industrially relevant methane conversions due to consecutive oxidation of produced hydrocarbons to CO and CO_2. A C_2-yield of 30% is regarded as the economically feasible limit for industrial realization of the process [2].

To improve the OCM selectivity a variety of less active oxidizing agents such as N_2O, CO_2, and H_2O have already been tested. This is not only for environmental reasons – N_2O and CO_2 are important greenhouse gases and their value added chemical transformation is highly desired [3] – but the major intention is the formation of more selective surface oxygen species on the catalyst. Clearly, the formation of electrophilic peroxo-species, which would favor the combustion of adsorbed hydrocarbons during

Comparison of Oxidizing Agents for the Oxidative Coupling of Methane over State-of-the-Art Catalysts, Langfeld K. et al.
Appl. Catal A: General 417-418 (2012) 145-152

2

OCM [4,5], is less probable when using these mild oxidizing agents because N_2O, CO_2, and H_2O, contrarily to O_2, can provide only one O atom for the catalyst reoxidation. The reaction mechanisms proposed for OCM are quite similar for each oxidizing agent and start with generation of surface active oxygen species from the oxidizing agent (Eqs. 1-3). Depending on the oxidizing agent, N_2 [6–9], CO [10–12], or H_2 [13] are formed as the by-product in these reaction steps. The reaction of O_2 (Eq. 1) is reported to pass a peroxo intermediate [5,14].

$$\tfrac{1}{2}\,O_2 + (\ ) \rightarrow (O) \qquad (1)$$
$$N_2O + (\ ) \rightarrow (O) + N_2 \qquad (2)$$
$$CO_2 + (\ ) \rightarrow (O) + CO \qquad (3)$$
$$H_2O + (\ ) \rightarrow (O) + H_2 \qquad (4)$$

The following (selective) reaction pathway is the oxygen-assisted CH_4 activation to form a methyl radical and a surface OH group [15,16]. The latter recombines to form gaseous H_2O and a vacancy to be reoxidized. Methyl radicals also recombine to form C_2H_6 which dehydrogenates to C_2H_4. Unselective pathways include the interaction of hydrocarbons and intermediates with electrophilic surface and gas phase species [17], such as mentioned surface peroxo-species [4], or gas phase O_2 [15].

One of the most promising and probably the best investigated [18] catalyst for OCM is Li-doped MgO [15,19–21]. However, a recent review [22] reveals numerous well-performing and promising catalyst compositions reported in literature so far. In the co-feed mode (simultaneously introducing CH_4 and O_2 into the reactor) C_2-yields up to 25-27% have been reported over $RbWO_4/SiO_2$ and $Bi_{1.5}Y_{0.3}Sm_{0.2}O_{3-\delta}$ catalysts, respectively [23,24]. High yields on less selective catalysts can also be obtained by improved reaction engineering [25]. For example, yields in the range of 17-23% were reported when operating in a membrane reactor with an oxygen-ion conducting $La_{0.8}Sr_{0.2}Co_{0.6}Fe_{0.4}O_{3-\delta}$ membrane separating the CH_4 and O_2 gas streams [26], or by alternating feed mode of CH_4 and O_2, e.g., over $Sr_{0.75}Na_{0.25}NiO_{3-\delta}$ or $SrNi_{0.75}Li_{0.25}O_{3-\delta}$ [27], even though applied perovskite-type and/or Ni-containing catalysts are commonly used for catalyzing partial or total oxidation pathways of methane. However, a major lack of so far published catalytic data is the poor comparability among studies by different authors. For instance, as can be seen in Tab. 1, reaction temperatures, CH_4/O_2 ratios, and space velocities cover a broad range and make assembled data difficult to compare. Other important data such as conversion of O_2 or stability with time-on-stream are often not given.

Besides the chemical composition, also the preparation method could provide a certain potential for optimizing the catalyst activity and C_2-yields. In recent studies, we could show that synthesis methods utilizing w/o-microemulsions [28] or cellulose filter papers [29] as structural templates for mixed metal oxides can significantly improve the catalytic properties of perovskite-type catalysts for oxidative methane activation as compared to conven-tional co-precipitation or sol-gel methods. The overall activity as well as the selectivity to C_2 products can be influenced.

The present study aims at the improvement of C_2 yields in the OCM reaction. Based on the elemental compositions and preparation recipes of best performing catalysts reported in literature this is intended to be realized by variation of the oxidizing agent and by applying cellulose templating (CT) as an alternative synthesis method to the respective method reported in literature. This study furthermore provides a direct comparison of catalytic performances of state-of-the-art catalysts reported in past literature.

2. Experimental

2.1. Catalyst Selection and Preparation

The catalysts investigated in the present study are listed in Tab. 1. They are selected according to their high C_2 yields in the OCM reaction as reported in current literature. In a recent study [29] we modified perovskites compositions towards high ability to oxidatively activate CH_4. With respect to their high activity and selectivity towards total methane combustion products these were employed for estimating the potential of N_2O to form more OCM selective oxygen species at temperatures > 823 K. Hereinafter, the catalysts are denoted with the elemental symbols of their metallic constituents without stochiometry but followed by (CT) or (lit) according to the cellulose templating or literature methods, respectively. For instance, the catalyst with the composition BaF_2(95 mol%)/Y_2O_3 prepared by the respective method reported in literature is labeled with BaY(lit).

For the preparation of CT-type catalysts, corresponding metal acetates and nitrates as well as ammonium salts of anionic precursors were dissolved in stochiometric amounts in deionized water. The solution (0.35 mol L^{-1}) was carefully dripped onto filter paper (Whatman 50, low ash) in the ratio of 1.7 mL g^{-1} liquid per filter paper. Subsequently, without drying, the impregnated filter papers were transferred into a preheated muffle oven (1273 K) and calcined for 3 h in air [29].

Other samples were synthesized by calcination of catalyst precursors prepared by co-precipitation/impregnation (NaBaSrTi, LiCeMg), incipient wetness impregnation (RbWSi, NaWSi, LiMg), citric acid sol-gel method (SrNaNi, SrNiLi, BiYSm) or calcination of precursor salt mixtures (BaY, LaCa, NdCa). Details of preparation recipes are given in the respective references listed in Tab. 1. All chemicals were purchased from Fluka, Roth, and Merck with a purity grade of >99% and were used without further purification.

Comparison of Oxidizing Agents for the Oxidative Coupling of Methane over State-of-the-Art Catalysts, Langfeld K. et al.
Appl. Catal A: General 417-418 (2012) 145-152

3

Table 1. Catalysts investigated in the present study and their performances in the OCM under different reaction conditions as reported in literature.

Catalyst	T (K)	$CH_4:O_2$:inert	GHSV ($mL\,g^{-1}\,h^{-1}$)	$X(CH_4)$ (%)	$S(C_2)$ (%)	Ref.
BaF_2(95 mol%)/Y_2O_3	1023	2.5:1:11	6000	36.1	62.1	[30]
Rb_2WO_4(0.3 mmol g^{-1})/SiO_2	1123	4.5:1	2000[a]	32	78	[23]
Na_2WO_4(0.3 mmol g^{-1})/SiO_2	1123	4.5:1	2000[a]	44	52	[23]
$NaMnO_4$(12.5 wt%)/MgO	1073	5:1:4	4800	28[b]	69	[31]
Na(0.32 g)/$BaSrTiO_3$	1073	2:1:2	6000[a]	47	51	[32]
Li(0.2 wt%)/MgO	923	21:1:28	6000	3.0	17.7	[15]
$SrCO_3$/$La_2(CO_3)_3$ (La:Sr = 2)	1153	10:1:0	219,800	15.8[b]	80.8	[33]
La(5 mol%)/CaO	1073	8:1:0	51,360	19.8	67.2	[34]
Nd(5 mol%)/CaO	1073	8:1:0	51,360	19.5	70.8	[34]
Li(5 mol%)/Ce(0.5 mol%)/MgO	1073	5:1:44	6000	21.7	64.0	[35]
$Bi_{1.5}Y_{0.3}Sm_{0.2}O_{3-\delta}$	1223	2:1:3	8955	42.4[b]	62.7	[24]
$Bi_{1.5}Y_{0.3}Sm_{0.2}O_{3-\delta}$	1173	Membrane reactor, 21% O_2/N_2 (oxygen side), 2% CH_4/He (methane side)		65.0	54.7	[36]
$Sr_{0.3}La_{0.7}MnO_x$	823	2:1:7	30,000	28.5[b]	<5	[29]
$Sr_{0.4}La_{0.6}Fe_{0.2}Co_{0.8}O_x$	823	2:1:7	30,000	27.4	<5	[29]

[a] h^{-1}.
[b] Limited by full O_2 conversion: $X(O_2) > 90\%$.

2.2. Catalyst Characterization

For a detailed physico-chemical characterization of the large amount and diversity of catalysts tested, we refer to the respective literature listed in Tab. 1 as the focus of this study is the catalytic testing. However, selected catalyst samples showing a strongly different catalytic behavior (see Fig. 4) were subjected to repeated structural analyses after the catalytic tests after 40 h in OCM feed with O_2 and N_2O as the oxidizing agents at temperatures between 973–1073 K. CO_2 has also been tested as a potential oxidizing agent, however, these experiments are described elsewhere [37]. The influences of the preparation method, the catalytic conditions or the nature of the oxidative agent thereon are discussed.

The specific surface areas of the catalyst samples were determined by N_2 adsorption at 77 K, using a Micromeritics 2375 BET apparatus equipped with a Vacprep 061 degasser. Before acquisition of the adsorption isotherm, the samples were first outgassed at 15 Pa and 393 K for 12 h, to ensure a clean and dry surface. The specific surface areas were calculated from the BET equation from adsorption data in the range of $p/p_0 = 0.05\text{-}0.3$.

Powder X-ray diffraction (XRD) measurements were conducted in order to get information about crystalline phases and crystallite size in the catalysts. The XRD patterns of catalyst samples were obtained using a STOE STADI-P transmission diffractometer with a focusing primary Ge(111) monochromator applying Cu Kα radiation (λ = 1.5406 Å) and a scanning angle (2θ) range of 10–90°.

A Hitachi S-4800 instrument with an EDAX Genesis EDX detector was used for scanning electron microscopy (SEM) studies. The samples were deposited on carbon tape. Images were acquired at 2 kV to optimize surface resolution, while energy dispersive X-ray spectroscopy (EDX) was carried out with an accelerating voltage of 15 kV.

2.3. Catalyst Testing

Catalytic tests on the OCM reaction were carried out in a multi-channel reactor system located at LIKAT (Rostock). This set-up consists of 48 plug flow fixed-bed quartz reactors with an inner diameter of 4 mm operating in parallel. The feed gas mixtures, as introduced one after the other at atmospheric pressure, comprised CH_4/air, CH_4/N_2O/Ar, and CH_4/CO_2/N_2 mixtures in stochiometric O/C = 1 ratio with regard to the OCM reaction while keeping the CH_4 concentration constant, i.e., $CH_4:O_2:N_2 = 2:1:4$, CH_4/N_2O/Ar = 2:2:3, and $CH_4:CO_2:N_2 = 2:2:3$. The catalyst grains (250–300 μm) were diluted with quartz sand (except for the respective reactors with lowest GHSV) and filled into each reactor. One empty reactor was chosen to account for the detection of gas phase reactions and analysis of educt gas composition was realized by a bypass line. An in-house developed flow restrictor equally distributed the total gas flow to the 48 reactors with a constant single reactor flow of 15 mL min^{-1}. A variation of space velocity was realized by using different amounts of catalysts in parallel operating reactors. Thus, using catalyst masses between 50 and 500 mg, gas hourly space velocities (GHSV) of 3,600–100,000 h^{-1} were adjusted. The catalysts were heated in Ar up to 973 K and then brought in contact with the reactant feed. For each oxidizing agent, reactor temperatures of 973, 1023, and 1073 K were adjusted. Each temperature was held for approx. 12 h corresponding to 3 measuring points of product gas composition.

The feed components and the reaction products were analyzed by an online gas chromatograph (Agilent 7890) equipped with PLOT/Q (for CO_2 and N_2O), AL/S (for hydrocarbons) and Molsieve 5 (for H_2, O_2, N_2, and CO) columns as well as flame ionization and thermal conductivity detectors. The conversion of CH_4 was calculated from the inlet and outlet concentrations of CH_4. The product selectivities were calculated on the product basis. The GC analysis started after the system had reached reaction temperature and was carried out sequentially for each individual reactor.

Comparison of Oxidizing Agents for the Oxidative Coupling of Methane over State-of-the-Art Catalysts, Langfeld K. et al.
Appl. Catal A: General 417-418 (2012) 145-152

4

Table 2. Specific surface areas of selected catalysts.

Catalyst	S_{BET} (m^2 g^{-1})	$S_{BET,lit}$ (m^2 g^{-1})	Ref.
NaWSi(lit)	1.2	–[a]	[23]
BaY(lit)	2.0	1.1	[30]
LiMg(lit)	0.1	37	[15]
LiMg(CT)	12.7	16[b]	[38]
SrLaFeCo(CT)	1.7	11.9	[29]

[a] Not published.
[b] Pure MgO. T_{cal} = 1323 K.

3. Results and Discussion

3.1. Catalyst Characterization

3.1.1. N_2 physisorption and X-ray Diffraction

Characterization results presented herein were selected according to the catalysts OCM behavior by employing the criteria as mentioned in section 2.2. Briefly, during OCM with O_2 at 1073 K, NaWSi(lit), LiMg(lit), and BaY(lit) provide highest C_2 selectivities around 40% at different degrees of methane conversion in the range of 30–50%. Contrarily, LiMg(CT) shows a C_2 selectivity of only 16% at the similar level of CH_4 conversion. The perovskite SrLaFeCo(CT) provides a methane conversion of 30%, which is limited by full O_2 conversion, at almost zero C_2 selectivity. Specific surface areas of these catalysts are listed in Tab. 2. The comparison with literature data shows that all catalysts provide a low surface area after long term catalytic tests in OCM reaction. Especially for LiMg(lit), LiMg(CT), and SrLaFeCo(lit) a dramatic difference is observed. For BaY(lit), low surface areas are explained by sintering effects during high temperature treatment [30] and it is assumed that this is also the reason for structural collapse of other catalysts investigated. Accordingly, the high surface area of LiMg(lit) was measured after a reaction time of 3 h at the low temperature of 923 K [15]. However, even though showing a lower C_2-selectivity in comparison to LiMg(lit), the structural stability of LiMg(CT) is remarkable and the sample keeps the relatively high surface area of > 12 m^2 g^{-1} even after long term reaction conditions.

Comparing the crystallographic data gained from XRD analysis over fresh and used catalysts reveals significant restructuring induced by being applied to OCM reaction for 40 h on stream; solely the LiMg samples are phase stable under the above conditions. Owing to the low Li loading the diffractograms of LiMg(lit) and LiMg(CT) (not shown) disclose phase-pure MgO according to powder diffraction file PDF 00-043-1022. The peak analysis according to Scherrer [39] gives an estimate of the mean crystallite sizes of 188 and 114 nm [40] for LiMg(lit) and LiMg(CT), respectively. This correlates well with the higher surface area of the CT sample and underlines the advantages of the cellulose template method for the synthesis of highly dispersed and structurally stable oxidic structures [38]. The BaY(lit) sample (see Fig. 1) comprises BaF_2
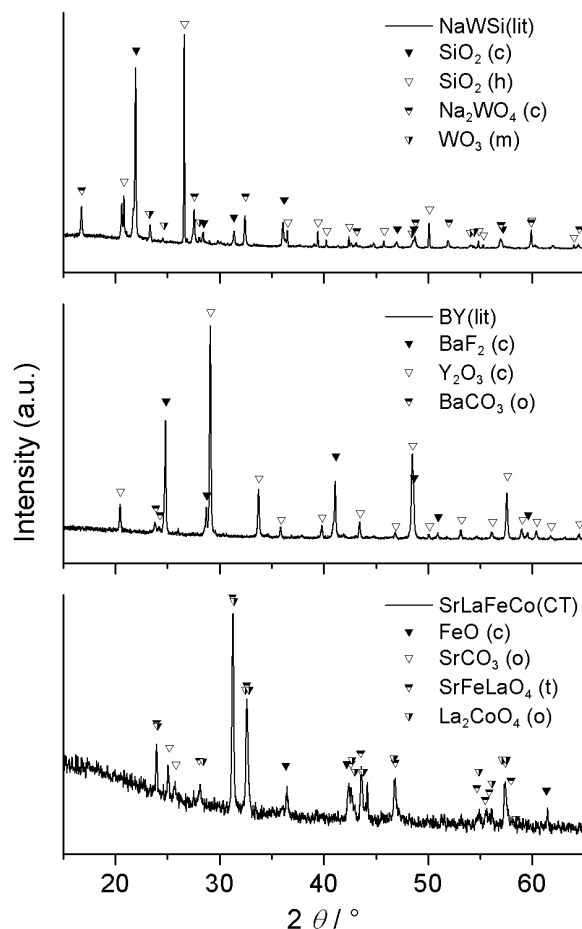

Figure 1. XRD patterns of NaWSi(lit), BaY(lit), and SrLaFeCo(CT) catalysts after use in OCM for 40 h on stream, reaction conditions as listed in section 2.3. Modifications are given in parenthesis: cubic (c), hexagonal (h), monoclinic (m), orthorhombic (o), tetragonal (t).

(PDF 00-085-1342) and Y_2O_3 (PDF 00-041-1105) phases and a small amount of $BaCO_3$ (PDF 00-044-1487). The stability of the precursor phases is reported in literature [30], however, the presence of a carbonate phase indicates the slow transformation of BaF_2 to $BaCO_3$ in the presence of CO_2, which is a by-product of OCM. This questions the stability of BaY(lit) at extended OCM reaction periods, although the formation of $BaCO_3$ could also be accelerated by the experiments using CO_2 in high concentration as the oxidizing agent [37].

The NaWSi(lit) catalyst comprises two different modifications of the SiO_2 support, namely cubic cristobalite (PDF 00-001-0438) and tetragonal quartz (PDF 00-033-1161), whereas in the original report only the christobalite phase is detected [23]. More importantly, a small amount of WO_3 (PDF 00-030-1387) can be identified by XRD, suggesting that Na_2WO_4 (PDF 00-012-0772) is unstable under the reaction conditions applied. The least structurally stable catalyst is SrLaFeCo(CT), which completely decomposes into FeO (PDF 00-001-1223), $SrCO_3$ (PDF 00-005-0418) as well as several binary and ternary mixed oxide phases,
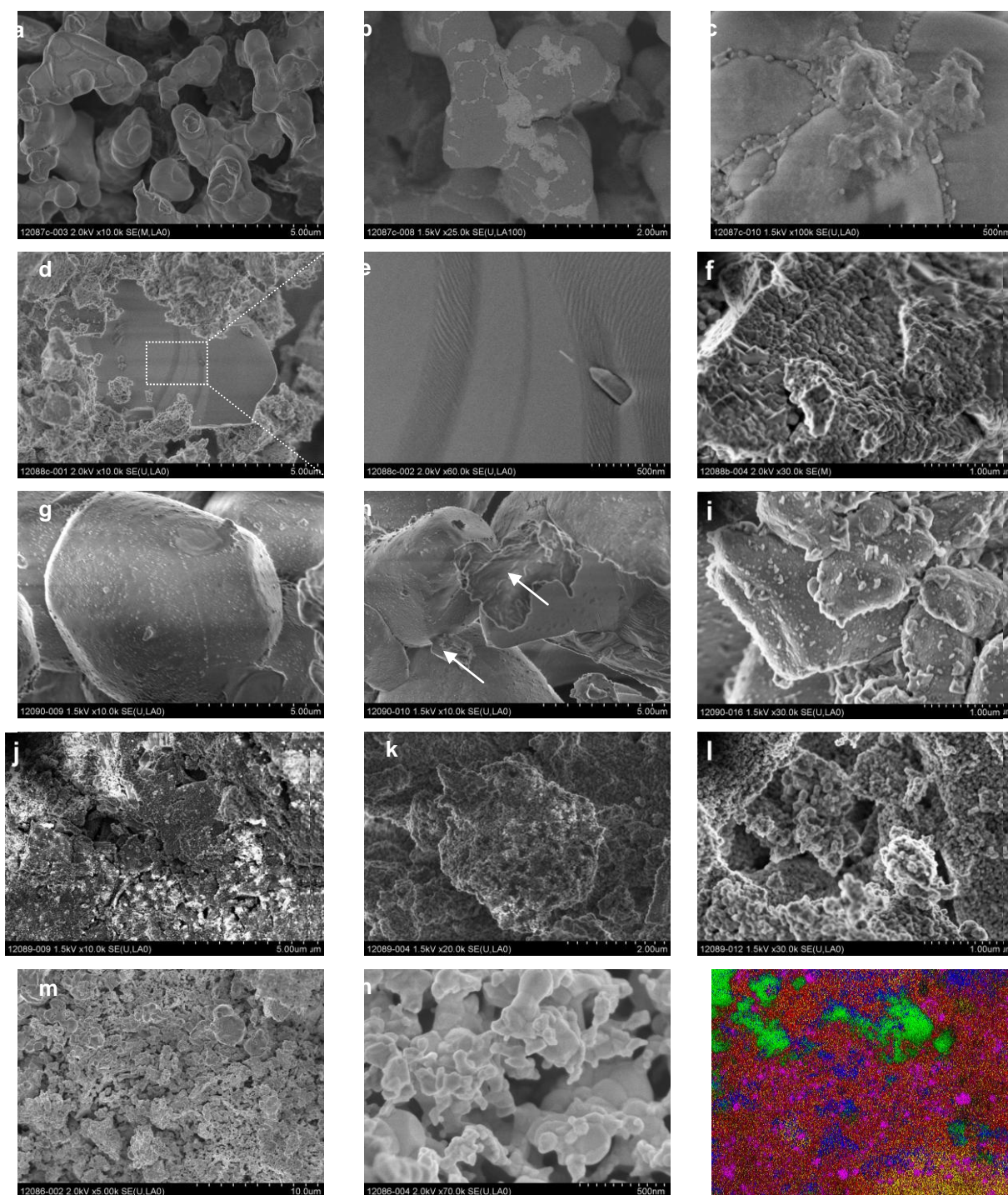
Comparison of Oxidizing Agents for the Oxidative Coupling of Methane over State-of-the-Art Catalysts, Langfeld K. et al.
Appl. Catal A: General 417-418 (2012) 145-152

5

Figure 2. SEM images of NaWSi(lit) (a-c), BaY(lit) (d-f), LiMg(lit) (g-i), LiMg(CT) (j-l), and SrLaFeCo(CT) (m-n) catalysts after use in OCM for 40 h on stream under varying reaction conditions. The elemental mapping of SrLaFeCo(CT) (o) shows section (m) and indicates enrichment of Sr (green), La (red), Fe (yellow), Co (magenta), and O (blue).

which are difficult to identify in detail. Although the ICSD database [41] provides numerous similar patterns containing the elements of the perovskite, the typical reflexes of $SrFeLaO_4$ (PDF 00-029-1305) and La_2CoO_4 (PDF 00-034-1081) are given as references. The signal-to-noise ratio detected in the diffraction patterns of the fresh SrLaFeCo(CT) (as can be taken from [29]) is lower compared to that of used SrLaFeCo(CT) depicted in Fig. 1. This may

demonstrate a loss of crystallinity, which is in line with the structural collapse of the material.

3.1.2. Scanning Electron Microscopy

The SEM and EDX analyses of the used catalysts are shown in Fig. 2. The porous structure of NaWSi(lit) (Fig.

Comparison of Oxidizing Agents for the Oxidative Coupling of Methane over State-of-the-Art Catalysts, Langfeld K. et al.
Appl. Catal A: General 417-418 (2012) 145-152

6

2a) is conserved from the porous SiO_2 support used for impregnation even after 40 h on OCM conditions. The elements are macroscopically well dispersed over the catalyst particles as pointed out by EDX analysis and backscattered SEM (Fig. 2b). Na_2WO_4 is dispersed on the smooth SiO_2 surface in 50–500 nm sized clusters (Fig. 2c). Traces of C are mainly located on the SiO_2 surface, whereas the W- and Na-rich areas are almost free of C. BaY(lit) (Fig. 2d) remains a physical mixture of plain shaped BaF_2 crystals (Fig. 2e) and Y_2O_3 (Fig. 2f), which provides a rough surface. In agreement with the phase analysis by XRD, the elemental mapping reveals the coherence of Ba and F, as well as Y and O. Traces of C can be detected on both BaF_2 and Y_2O_3 materials.

The LiMg catalysts show clear differences in their microstructure. LiMg(lit) conserved the ~5 μm sized spherical MgO particles with smooth surfaces (Figs. 2g and h), whereas LiMg(CT) appears less ordered and provides rough surfaces (Figs. 2j-l) in agreement with the higher specific surface area owing to the CT method (Tab. 2). However, the latter misses the typical cellulose templated structure observed for other mixed oxides [29], which is probably due to sintering processes during reaction. On both samples Li cannot be detected by EDX due to the low loading of 0.2 wt% and the low atomic mass of Li. However, both samples provide a strong C signal, which is even more pronounced on the LiMg(CT) sample. It is also confirmed by optical analysis of used catalysts, whose colors are grey and white for LiMg(CT) and LiMg(lit) samples, respectively. On LiMg(lit) carbon is present in the form of bigger flakes (Figs. 2g and h, arrows), whereas on the CT sample it appears to be more homogeneously distributed. The latter fact may hint towards C to be partly present as an artifact of the cellulose template. The primary particle size of MgO crystallites in both samples is in the range of 100-200 nm (Figs. 2i and l) in agreement with XRD analysis.

The most drastic structural collapse is observed for the SrLaFeCo(CT) catalyst, as indicated by the XRD analysis. The nicely adapted cellulose structure (as had been observed in [29]) is completely destroyed and sintered to form a less porous microstructure (Fig. 2m and n). The metallic constituents of the homogeneously substituted perovskite segregated to form crystallites and clusters of varying composition, mainly oxides and carbonates as illustrated in the element map (Fig. 2o). The average chemical composition as determined by EDX, however, still represents the stochiometry of the perovskite (Sr: 21.6 at%, La: 30.6 at%, Fe: 9.6 at%, Co: 38.2 at%). Only small amounts of C can be detected on the SrLaFeCo(CT) sample.

3.2. Catalytic Testing

3.2.1. Li$_2$O/MgO based catalysts

The catalytic performances of pure as well as Zr and Ce doped Li_2O/MgO catalysts are shown in Tab. 1. The stability is given as the temporal change of absolute activity

Table 3. Catalytic performances of L$_2$O/MgO-based catalysts in the reactions of CH_4 with O_2 and N_2O, respectively, (O/C = 1) at 1073 K and GHSV 3,600 h^{-1}.

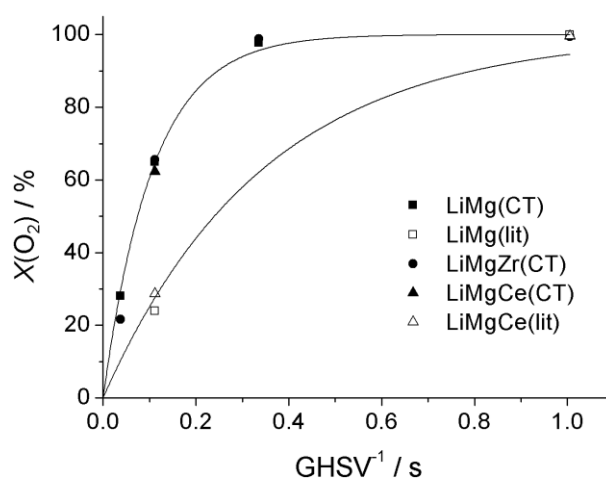| Catalyst	Oxidizing agent	$X(CH_4)$ (%)	$S(C_2)$ (%)	$\Delta X/\Delta t$ (% h^{-1})
LiMg(lit)	O_2	41.4	37.3	−0.33
	N_2O	9.0	55.2	−0.08
LiMg(CT)	O_2	28.1	12.9	−0.45
	N_2O	27.0	9.7	+0.02
LiMgZr(CT)	O_2	27.4	15.2	−0.38
	N_2O	30.6	41.7	−0.03
LiMgCe(lit)	O_2	43.0	37.0	−0.01
	N_2O	34.3	41.9	−0.01
LiMgCe(CT)	O_2	40.3	28.6	−0.08
	N_2O	33.7	36.4	+0.04

Figure 3. Conversions of O_2 in the OCM over LiMg-based catalysts at 1073 K.

in terms of CH_4 conversion dX/dt within 10 h on stream under the respective reaction conditions. In general, the use of O_2 as the oxidizing agent leads to higher conversions of CH_4 than N_2O except for LiMgZr(CT). Full conversion of O_2 and N_2O, respectively, at the GHSV of 3600 h^{-1} is observed in each case. N_2O is totally converted except over LiMg(lit). It is seen that the CT catalysts provide lower conversions of CH_4 than the catalysts prepared by recipes from literature [15,35]. With regard to the full conversion of O_2, this can be directly correlated to the lower selectivity because the total oxidation of CH_4 consumes more O_2 than the selective OCM. The doped CT catalysts provide a higher C_2 selectivity and also a higher stability over the pure LiMg(CT). ZrO_2 and CeO_2 are known as red-ox promotors and structural stabilizers, which can enhance the catalytic performance of active components [42].

Also the oxidizing agent has a remarkable impact on the stability of the samples. O_2 leads to a rapid activity loss in most cases, which is well-known for Li_2O/MgO catalysts [19,43]. Contrarily, the use of N_2O apparently prevents the deactivation by O_2. In some cases even an increase in activity with time on stream was observed ($\Delta X/\Delta t$ >0). The lower oxidation strength of N_2O also lowers the areal rate of CH_4 conversion (see Tab. 3). Moreover, the formation of more selective O species on the catalyst surface when using

Comparison of Oxidizing Agents for the Oxidative Coupling of Methane over State-of-the-Art Catalysts, Langfeld K. et al.
Appl. Catal A: General 417-418 (2012) 145-152

7

Table 4. Catalytic performances of alkaline tungstate catalysts in the reactions of CH_4 with O_2 and N_2O, respectively, (O/C = 1) at 1073 K and GHSV 3,600 h^{-1}.

Catalyst	Oxidizing agent	$X(CH_4)$/%	$S(C_2)$/%	$\Delta X/\Delta t$/% h^{-1}
NaWSi(lit)	O_2	4.9	14.2	−0.05
	N_2O	4.3	83.4	−0.16
NaWSi(CT)	O_2	32.1	25.5	+0.19
	N_2O	21.3	49.5	−0.05
RbWSi(lit)	O_2	29.7	45.3	−0.12
	N_2O	3.8	73.5	−0.12
RbWSi(CT)	O_2	31.8	29.9	+0.06
	N_2O	27.0	42.1	−0.03

Table 5. Catalytic performances of earth alkaline and lanthanide oxides in the reactions of CH_4 with O_2 and N_2O, respectively, (O/C = 1) at 1073 K and GHSV 3,600 h^{-1}.

Catalyst	Oxidizing agent	$X(CH_4)$ (%)	$S(C_2)$ (%)	$S(C_2)^a$ (%)	$\Delta X/\Delta t$ (% h^{-1})
SrLa(lit)	O_2	32.6	18.9	22.1	−0.19
	N_2O	26.7	20.0	28.5	−0.01
SrLa(CT)	O_2	37.5	22.2	29.1	−0.07
	N_2O	29.8	26.8	31.1	+0.02
LaCa(lit)	O_2	35.9	16.7	21.4	−0.01
	N_2O	29.9	24.3	32.1	−0.01
LaCa(CT)	O_2	28.8	1.07	9.4	+0.06
	N_2O	27.5	18.5	19.9	−0.01
NdCa(lit)	O_2	32.9	12.0	20.9	−0.05
	N_2O	30.2	28.4	28.6	+0.02
NdCa(CT)	O_2	33.5	13.4	21.1	±0
	N_2O	29.8	30.6	35.0	+0.02

^{a} GHSV 32,000 h^{-1}.

N_2O as the oxidizing agent lowers the local heat production since the reaction enthalpy for selective OCM reaction is lower than that of the CH_4 combustion. Thus it is assumed that the hot spot in the catalyst bed is more pronounced in the OCM with O_2, which could be one reason for the differences in deactivation behavior. Accordingly, the thermally induced deactivation of the LiMg(CT) catalyst in OCM with O_2, i.e., sintering and/or evaporation of Li [18], is only 0.04 % h^{-1} at 1023 K and 0.002 % h^{-1} at 973 K, even though full O_2 conversion is obtained in each case.

In this view the origin of the lower stabilities and the lower C_2 selectivities obtained over the CT catalysts are assumed in their relatively high surface area leading to heat transfer limitations, which could favor secondary combustion of formed C_2 products [44] and thus explain the lower selectivity observed on these samples. The conversions of O_2 at 1073 K are compared in Fig. 3 and it is seen that the global rates are by a factor of approx. 2 higher on the CT catalysts irrespective of the doping, which apparently only affects the product selectivities.

3.2.2. Tungstate catalysts

Methane conversions, C_2 selectivities as well as catalytic stability of NaWSi and RbWSi samples are shown in Tab. 4. The CT method leads to slightly higher conversions in the OCM with O_2. Generally, OCM activity with N_2O as

the oxidizing agent is exceeding that of OCM with O_2. The higher activity of CT prepared catalysts is attributed to the fine dispersion of tungstate ions over the catalyst bulk and surface as a result of the CT method. This provides an ideal distribution of the metal cations on a molecular level in the salt solutions prior to the impregnation of the template [45]. Instead, the incipient wetness impregnation reported in literature [23] yields agglomerates of alkaline tungstates on the SiO_2 surface (Fig. 2b and c).

Contrarily to the Li_2O/MgO based catalysts, the tungstates tend to be more stable in the O_2 containing feed and deactivate in the OCM feed with N_2O. Especially for the CT catalysts, a gain in activity is observed for the reaction with O_2. Even more importantly the C_2 selectivity also increases with time-on-stream indicating that the maximum performance of these catalysts is not equilibrated even after 40 h reaction time. The loss of activity of the NaWSi(lit) sample can possibly be attributed to the decomposition of the Na_2WO_4 phase to WO_3 (Fig. 1).

3.2.3. Earth alkaline and lanthanide oxides

The catalytic performance of earth alkaline and lanthanide oxide catalysts tested in this study is assembled in Tab. 5. At 1073 K and GHSV of 3,600 h^{-1}, all catalysts showed full O_2 conversion as it is also valid for the almost tenfold lower contact time (GHSV 32,000 h^{-1}). The CH_4 conversion is lower for N_2O than O_2 as the oxidizing agent and almost unaffected by contact time in this regime free of oxidative compounds. However, the C_2 selectivity significantly increases with decreasing contact times. From that, we suggest that the catalytic performance shown in Tab. 5 is far from optimum conditions. As shown in Tab. 1, a CH_4:O_2 feed ratio > 2 is frequently observed for this class of catalysts. The catalysts of this group are very stable under the reaction conditions applied.

Although full conversion of the oxidizing agent is also observed in all experiments with N_2O, the conversions of CH_4 are higher in the presence of O_2 regardless the same C/O feed ratio in these comparative experiments and the higher C_2 selectivities obtained with N_2O. However, with regard to the secondary degradation of C_2 products as mentioned above, the latter might be the result of a slower overall reaction and not necessarily points at a different (more selective) O species formed by N_2O. In each case it is assumed that even at the short contact times significant coking occurs on these highly active catalysts. Unfortunately, shorter contact times have not been realized in the experimental program. The CT method provides slight advantages in terms of CH_4 conversion and C_2 selectivity for SrLa and NdCa samples, whereas the preparation method reported in literature [34] appears to be the better choice in case of the LaCa catalyst.

Comparison of Oxidizing Agents for the Oxidative Coupling of Methane over State-of-the-Art Catalysts, Langfeld K. et al.
Appl. Catal A: General 417-418 (2012) 145-152

8

Table 6. Catalytic performances of halogenide containing catalysts in the reactions of CH_4 with O_2 and N_2O, respectively, (O/C = 1) at 1073 K and GHSV 3,600 h^{-1}.

Catalyst	Oxidizing agent	$X(CH_4)$ (%)	$S(C_2)$ (%)	$\Delta X/\Delta t$ (% h^{-1})
BiYSm(lit)	O_2	34.7	23.5	+0.12
	N_2O	27.0	23.0	±0
BiYSm(CT)	O_2	27.5	5.0	−0.03
	N_2O	23.5	3.3	−0.01
NaMnMg(lit)	O_2	33.7	22.4	+0.09
	N_2O	16.7	29.3	−0.28
NaMnMg(CT)	O_2	28.6	0.7	+0.19
	N_2O	22.6	1.4	−0.01
BaY(lit)	O_2	45.4	40.7	+0.05
	N_2O	22.9	67.0	−0.25
BaY(CT)	O_2	27.4	8.7	−0.01
	N_2O	21.8	9.3	−0.18
NaBaSrTi(lit)	O_2	6.7	9.3	−0.73
	N_2O	2.9	0.0	−0.17
NaBaSrTi(CT)	O_2	28.1	0.0	−0.09
	N_2O	26.4	0.0	−0.02

3.2.4. BiYSm, NaMnMg, and halogenide containing catalysts

Catalytic data of halogenide containing catalysts as well as the NaMnMg and BiYSm samples are listed in Tab. 6. In general, the reaction with N_2O is slower as compared to O_2. However, for the BiYSm catalysts C_2 selectivities are lower at the lower conversions of CH_4 indicating that active sites (re)generated by N_2O are less selective than those (re)generated by O_2. A very poor performance is observed for the NaMnMg(CT) sample, which provides lowest C_2 selectivities. It suggests that highly oxidizing permanganate ions are reduced to $Mn^{2+/3+}$ during the CT synthesis and released oxygen is consumed for the combustion of the cellulose template. Instead the impregnated NaMnMg(lit) catalyst [31] provides drastically improved conversions of CH_4 and higher selectivities to C_2 products in the OCM with O_2. The BaY samples show highest yields observed in this study and the use of N_2O increases the C_2 selectivity, however, at lower conversion of CH_4 making it difficult to distinguish whether this effect is due to secondary combustion of C_2 products or due to catalyst improvement. Full conversion of the oxidizing agent is observed in each experiment listed in Tab. 6. BiYSm(lit), BaY(lit), and NaMnMg catalysts increase in activity with time-on-stream whereas all other samples show a stable catalytic performance or deactivate. BaY catalysts are unstable in N_2O suggesting that a high oxidative potential is required to maintain the catalytic activity similar to the observation of the low C_2 selectivity over the reduced NaMnMg(CT) sample..

A very poor catalytic performance in terms of OCM is observed for the NaBaSrTi catalysts. Zero selectivity to C_2 products is found in a broad range of reaction conditions, the low C_2 selectivity of NaBaSrTi(lit) in O_2 is overshadowed by a rapid activity loss. Regarding the poor performance of these catalysts in the present study, the high C_2 yield reported [32], however, under slightly different reaction conditions, is difficult to comprehend. Instead, the

high selectivities to CO_2 observed are in full agreement with the expected product spectrum for a perovskite-type catalyst [46].

The preparation method appears to be highly important for this group of catalysts. BiYSm and BaY catalysts provide a lower conversion of CH_4 when prepared via CT, which is a result of the drastically lowered C_2 selectivity as found for the Li_2O/MgO type catalysts. Similarly, the higher activity as a result of higher surface areas of CT samples is assumed to induce hot spots in the catalyst bed, which lower the C_2 selectivity and also the catalyst stability. For NaBaSrTi this effect is most obvious and the amenity of the CT method over citric acid sol gel synthesis is clearly visible [29] when C_2 selectivity is no object.

3.2.5. Perovskite reference samples

Perovskite-type oxides is a class of catalysts covering excellent materials for total oxidation of hydrocarbons with high selectivity to CO_2 [46]. In the present study selected samples showing a high CH_4 combustion performance with O_2 [29] were additionally tested in the reaction with N_2O. Although the lattice structure is not stable under the reaction conditions applied as shown for SrLaFeCo(CT) in the catalyst characterization section the catalysts tested show a very high and stable catalytic performance (Tab. 7) with a high selectivity to CH_4 combustion. The full conversion of O_2 and N_2O is found even at the lower reaction temperature of 1023 K and higher GHSV of 32,000 h^{-1}. Lower conversions of CH_4 when using N_2O are a result of higher selectivities to CO_2 obtained over these catalysts.

Furthermore, it is very interesting to note that trace amounts of C_2 products are detected when using this mild oxidizing agent. The amounts of C_2 products are even higher at the initial period of reaction and decrease with time-on-stream in parallel to the degradation of the perovskite lattice. It suggests that the initial well ordered structure, which brings up C_2 selectivities of up to 2%, has a certain, however limited, potential for OCM catalysis.

Table 7. Catalytic performances of perovskite catalysts in the reactions of CH_4 with O_2, CO_2, and N_2O, respectively, at 1073 K and GHSV 3,600 h^{-1}.

Catalyst	Oxidizing agent	$X(CH_4)$ (%)	$S(C_2)$ (%)	dX/dt (% h^{-1})
SrLaMn(CT)	O_2	28.8	0.0	−0.01
	N_2O	24.6	0.7	±0
SrLaFeCo(CT)	O_2	30.7	0.0	−0.03
	N_2O	24.3	0.1	−0.03

Comparison of Oxidizing Agents for the Oxidative Coupling of Methane over State-of-the-Art Catalysts, Langfeld K. et al.
Appl. Catal A: General 417-418 (2012) 145-152

9

3.3. Relationship between catalyst composition and their performance in OCM

The comparison of oxidizing agents for the OCM over state-of-the-art catalysts indicates that N_2O could contribute to the solution of the C_2 selectivity problem. The total activities are lower when using N_2O as the oxidizing agent, however, accompanied by higher selectivities to ethylene and ethane (Fig. 4). It is in agreement with the fact that N_2O is a mild and less reactive oxidizing agent, whereas O_2 is highly reactive and more rapidly reoxidizes the catalyst surface. The higher selectivities observed at the lower conversions when using N_2O, however, can also be explained by reaction kinetics. Decreasing S/X-trajectories are an indicator for a Wheeler type III reaction network of product formation and consecutive product degradation [47] as it is suggested for the OCM [17]. An increased microkinetic selectivity can only be determined at iso-conversion, i.e., by variation of GHSV. Unfortunately, several catalysts turned out to be too reactive thus providing full conversion of O_2 and N_2O in the whole range of GHSVs adjusted (e.g., SrLa, LaCa, NdCa). S/X data obtained in this regime is hard to compare. The statistical analysis of the entire dataset, however, reveals a remarkable improvement of the C_2 selectivity. In the range of CH_4 conversions between 25-35%, which comprises roughly 120 experimental data points of the entire dataset and corresponds to the upper limit of N_2O reactivity data, the increase of the average C_2 selectivity is + 11.1%. The superior N_2O performance can be due to the fact that the formation of gas-phase methyl peroxo species is strongly suppressed in the absence of gas-phase O_2. Such species are considered as precursors of gas-phase CO_2 [22]. Additionally, it is concluded that the superior performance of N_2O compared to O_2 is due to the formation of different adsorbed oxygen species upon catalyst reoxidation as previously reported for selective oxidation of low alkanes with N_2O and O_2 [4,5,48]. Mono-atomic species are the only species formed from N_2O, while bi-atomic oxygen species originate additionally from O_2. The former species selectively convert CH_4 to C_2H_6, while the latter ones are responsible for non-selective reaction products (CO and CO_2). As suggested previously [5] for the OCM reaction over Na/CaO, the relative ratio of bi-atomic to mono-atomic adsorbed species is influenced by the concentration of anion vacancies, which are active sites for O_2 adsorption. The higher the concentration of anion vacancies is, the lower is the ratio and the higher the C_2-selectivity is achieved. Such vacancies are created upon doping of CaO with Na_2O in the range of formation of solid solutions.

With regard to the CT method as an alternative approach for catalyst preparation it turns out that these catalysts in most cases are in parts drastically inferior to the samples prepared via the respective methods reported in literature. One reason could be the higher surface areas obtained, which increase the global reactivity to create hot spots in the catalyst bed and finally accelerate the combus
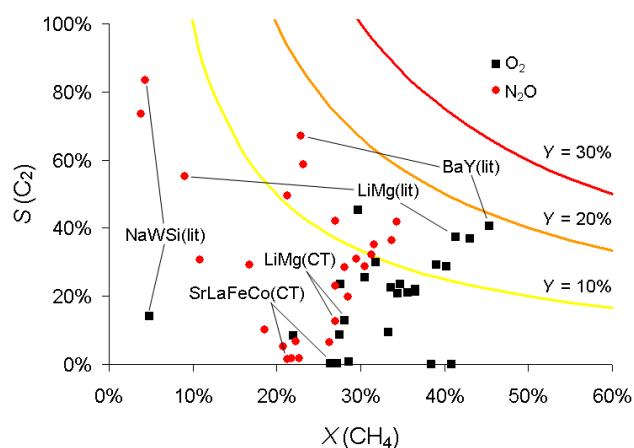

Figure 4. S/X-plot of catalytic performances obtained for all catalysts in the OCM with O_2 and N_2O at 1073 K. The plot contains data representing the highest C_2 yields obtained by variation of GHSV.

tion of C_2 reactants and products. Another reason could be the phase composition and hierarchical structure, which is, e.g, not BaF_2/Y_2O_3 in the BaY(CT) sample and not Na_2WO_4/SiO_2 in the NaWSi(CT) sample. Instead, various highly dispersed bulk mixed oxide phases are formed from the homogeneous mixture of precursor ions used for cellulose impregnation, which apparently is detrimental to the catalytic performance.

The last point to be mentioned is that the recipes reported in literature not in each case produce a valuable OCM catalyst. Especially for NaBaSrTi(lit), which is reported to provide a C_2 yield of almost 25% under reaction conditions similar to those applied in the present study [32], a poor catalytic performance with almost zero C_2 selectivity is found, which agrees with the typically observed high total oxidation performance of perovskite type catalysts [46]. The best catalyst identified under similar reaction conditions are BaY(lit), LiMg(lit), and LiMgCe(lit) giving yields of C_2 products close to 20%. The fact that the industrially relevant range of 30% is not attained must be referred to non-optimized reaction conditions, i.e., molar composition of the feed. As can be seen from Tab. 1, the molar ratio of $CH_4:O_2$ often exceeds the stochiometric value of 2, whereas the addition of an inert diluting agent is frequently omitted. Both factors could contribute to an improved catalytic performance.

4. Conclusion

The present study underlines that besides the chemical composition also the synthesis strategy is a crucial factor for success in terms of high C_2 yields in the OCM reaction. Catalyst recipes and trends in catalytic performances reported in literature could be reproduced in most cases. High surface areas obtained with the cellulose templating method can favor non-selective consecutive oxidation of primarily formed ethane to carbon oxides. The

Comparison of Oxidizing Agents for the Oxidative Coupling of Methane over State-of-the-Art Catalysts, Langfeld K. et al.
Appl. Catal A: General 417-418 (2012) 145-152

10

contribution of the latter reaction can be reduced when using nitrous oxide compared to oxygen as the oxidizing agent. As a result higher C_2 selectivities are achieved even at iso-conversion of methane. The superior performance of nitrous oxide is attributed to the nature of oxygen species formed upon catalyst reoxidation.

Acknowledgements

References

[1]   G.E. Keller, M.M. Bhasin, J. Catal. 73 (1982) 9-19.
[2]   J.C.W. Kuo, C.T. Kresge, R.E. Palermo, Catal. Today 4 (1989) 463-470.
[3]   E.V. Kondratenko, O. Ovsitser, Angew. Chem. Int. Ed. 47 (2008) 3227-3229.
[4]   U. Zavyalova, M. Geske, R. Horn, G. Weinberg, W. Frandsen, M. Schuster, R. Schlögl, ChemCatChem 3 (2011) 949-959.
[5]   E.V. Kondratenko, O.V. Buyevskaya, M. Soick, M. Baerns, Catal. Lett. 3-4 (1999) 153-159.
[6]   E.N. Voskresenskaya, L.I. Kurteeva, G.G. Pervyshina, A.G. Anshits, Catal. Today 24 (1995) 277-279.
[7]   G.M. Pajonk, T. Manzalji, Appl. Catal. A 108 (1994) 41-51.
[8]   H. Yamamoto, H.Y. Chu, M.T. Xu, C.L. Shi, J.H. Lunsford, J. Catal. 142 (1993) 325-336.
[9]   K. Otsuka, T. Nakajima, J. Chem. Soc., Faraday Trans. I 83 (1987) 1315-1321.
[10]   K. Aika, T. Nishiyama, J. Chem. Soc., Chem. Commun. (1988) 70-71.
[11]   C. Chen, Y. Xu, G. Li, X. Guo, Catal. Lett. 42 (1996) 149-153.
[12]   S. Wang, Z.H. Zhu, Energy & Fuels 18 (2004) 1126-1139.
[13]   X. Li, K. Tomishige, K. Fujimoto, Catal. Lett. 36 (1996) 21-24.
[14]   N.X. Lu, G. Fu, X. Xu, H.L. Wan, J. Chem. Phys. 128 (2008) 034702.
[15]   T. Ito, J. Wang, C.H. Lin, J.H. Lunsford, J. Am. Chem. Soc. 107 (1985) 5062-5068.
[16]   L.M. Aparicio, S.A. Rossini, D.G. Sanfilippo, J.E. Rekoske, A.A. Trevino, J.A. Dumesic, Ind. Eng. Chem. Res. 30 (1991) 2114-2123.
[17]   L. Mleczko, M. Baerns, Fuel Proc. Technol. 42 (1995) 217-248.
[18]   S. Arndt, G. Laugel, S. Levchenko, R. Horn, M. Baerns, M. Scheffler, R. Schlögl, R. Schomäcker, Catal. Rev. - Sci. Eng. 53 (2011) 424-514.
[19]   S. Arndt, U. Simon, S. Heitz, A. Berthold, B. Beck, O. Görke, J.-D. Epping, T. Otremba, Y. Aksu, E. Irran, G. Laugel, M. Driess, H. Schubert, R. Schomäcker, Top. Catal. 54 (2011) 1266-1285.
[20]   Y. Kuo, F. Behrendt, M. Lerch, Z. Phys. Chem. 221 (2007) 1017-1037.
[21]   P. Myrach, N. Nilius, S.V. Levchenko, A. Gonchar, T. Risse, K. Dinse, L.A. Boatner, W. Frandsen, R. Horn, H. Freund, R. Schlögl, M. Scheffler, ChemCatChem 2 (2010) 854-862.
[22]   E.V. Kondratenko, M. Baerns, in:, G. Ertl, H. Knözinger, F. Schüth, J. Weitkamp (Eds.), Handbook of Heterogeneous Catalysis, Wiley VCH, 2008, pp. 3010-3023.
[23]   A. Palermo, J.P. Holgado Vázquez, R.M. Lambert, Catal. Lett. 68 (2000) 191-196.

[24]   Y. Zeng, F.T. Akin, Y.S. Lin, Appl. Catal. A 213 (2001) 33-45.
[25]   H.R. Godini, H. Arellano-Garcia, M. Omidkhah, R. Karimzadeh, G. Wozny, Ind. Eng. Chem. Res. 49 (2010) 3544-3552.
[26]   Y. Zeng, Y.S. Lin, S.L. Swartz, J. Membr. Sci. 150 (1998) 87-98.
[27]   Y.I. Pyatnitskii, A.I. Bostan, L.N. Raevskaya, S.A. Nedil'ko, A.G. Dzyaz'ko, E.G. Zen'kovich, Theor. Exp. Chem. 41 (2005) 117-121.
[28]   K. Langfeld, E.V. Kondratenko, O. Görke, R. Schomäcker, Catal. Lett. 141 (2011) 772-778.
[29]   K. Langfeld, R. Marschner, B. Frank, R. Schomäcker, ChemCatChem 3 (2011) 1354-1358.
[30]   C.T. Au, X.P. Zhou, Y.W. Liu, W.J. Ji, C.F. Ng, J. Catal. 174 (1998) 153-163.
[31]   J.A. Sofranko, J.J. Leonard, C.A. Jones, A.M. Gaffney, H.P. Withers, Catal. Today 3 (1988) 127-135.
[32]   Z. Fakhroueian, F. Farzaneh, N. Afrookhteh, Fuel 87 (2008) 2512-2516.
[33]   H. Mimoun, A. Robine, S. Bonnaudet, C.J. Cameron, Appl. Catal. 58 (1990) 269-280.
[34]   V.H. Rane, S.T. Chaudhari, V.R. Choudhary, J. Chem. Technol. Biotechnol. 81 (2006) 208-215.
[35]   R.L.P. Gonçalves, F.C. Muniz, F.B. Passos, M. Schmal, Catal. Lett. 135 (2010) 26-32.
[36]   F.T. Akin, Y.S. Lin, Catal. Lett. 78 (2002) 239-242.
[37]   K. Langfeld, PhD thesis (submitted), Technical University of Berlin.
[38]   A.N. Shigapov, G.W. Graham, R.W. McCabe, H.K. Plummer Jr, Appl. Catal. A 210 (2001) 287-300.
[39]   P. Scherrer, Gött. Nachr. 2 (1918) 98-100.
[40]   Note that this is only a rough estimate as the Scherrer equation is valid only for crystallite diameters below 100 nm.
[41]   Inorganic Crystal Structure Database, URL: http://icsd.fkf.mpg.de/ (Oct 2011).
[42]   A. Mastalir, B. Frank, A. Szizybalski, H. Soerijanto, A. Deshpande, M. Niederberger, R. Schomäcker, R. Schlögl, T. Ressler, J. Catal. 230 (2005) 464-475.
[43]   S. Arndt, Stability of lithium doped magnesium oxide and zinc oxide catalysts for the conversion of natural gas, Technical University of Berlin, 2011.
[44]   B. Frank, A. Dinse, O. Ovsitser, E.V. Kondratenko, R. Schomäcker, Appl. Catal. A 323 (2007) 66-76.
[45]   E.V. Kondratenko, V. Gölden, S. Sokolov, ChemCatChem 2 (2010) 633-635.
[46]   L.G. Tejuca, J.L.G. Fierro, Properties and applications of perovskite-type oxides, Marcel Dekker, New York, 1993.
[47]   A. Wheeler, Adv. Catal. 3 (1951) 249–327.
[48]   X. Rozanska, E.V. Kondratenko, J. Sauer, J. Catal. 256 (2008) 84-94.